RSC Advances

PAPER

View Article Online
View Journal | View Issue

Cite this: *RSC Adv.*, 2021, **11**, 501

Cytochrome c-multiwalled carbon nanotube and cobalt metal organic framework/gold nanoparticle immobilized electrochemical biosensor for nitrite detection

Shan Huang,[a] Ming Lu[b] and Lei Wang*[c]

Based on cytochrome c-multiwalled carbon nanotubes (Cyt c-MWCNTs) and cobalt metal–organic frameworks/gold nanoparticles (Co-MOFs/AuNPs), an electrochemical biosensor was proposed for the detection of nitrite. Herein, Co-MOFs and AuNPs were immobilized on gold electrodes *via* surface layer assembly. Their advantages including large surface area and high conductivity provided an excellent platform for the immobilization of Cyt c-MWCNTs. Cyt c-MWCNTs were prepared *via* electrostatic adsorption and possessed good biocompatibility and superior electrocatalytic activity towards nitrite. Notably, MWCNTs and AuNPs could provide a good microenvironment for the electron transfer of Cyt c, which further significantly promoted the dispersion of MWCNTs. All of the above features led to outstanding electrochemical performance and achieved signal amplification for nitrite detection. Therefore, the biosensor displayed a linear range from 0.005 μmol L^{-1} to 1000 μmol L^{-1} with a detection limit of 0.0044 μmol L^{-1} for nitrite detection. In addition, the designed biosensor exhibited excellent selectivity and could be applied in real samples.

Received 10th November 2020
Accepted 11th December 2020

DOI: 10.1039/d0ra09551f

rsc.li/rsc-advances

1. Introduction

Nitrite, a class of inorganic compounds, is widespread in food, drinking water and the environment because of its universality as a food additive and corrosion inhibitor in agriculture and industry.[1–3] Nevertheless, excessive intake of nitrite reduces the blood oxygen delivery capacity and generates strong carcinogens, which causes diseases in human health such as spontaneous abortion, birth defects and blue baby syndrome.[4–7] Therefore, it is of great practical significance to detect nitrite. In the last few years, several methods have been developed for nitrite detection such as spectrophotometry,[8] chromatography[9,10] and fluorescence analysis.[11] Undeniably, they can meet the requirements of accurate and sensitive detection. However, they also have some disadvantages including limited analytical samples, and being unsuitable for rapid batch testing and real-time field testing, which hinder their further development of nitrite detection.[12,13] Thus, seeking an alternative method to detect nitrite is necessary.

Recently, electrochemical sensors are rapidly developing due to fast response, convenient operation, high sensitivity, low cost and easy miniaturization.[14] Some novel electrochemical sensors based on nanocomposites have been reported to detect nitrite. For example, Li *et al.* constructed an electrochemical sensor based on Au nanoparticles/MoS_2 nanosheets for nitrite detection, which can meet the requirements of application research.[15] However, the selectivity of these electrochemical sensors based on nanocomposites needs to be improved. In this connection, it is urgent to explore a highly selective biomolecule.

Cytochrome c (Cyt c), as an enzyme, is favored by researchers and used in the electrochemical biosensor of nitrite. In addition, Cyt c plays the role of oxidoreductase in organism and is responsible for electron transfer.[16,17] However, it has been reported that electron transfer between electrode and Cyt c is difficult to achieve, because the active center of the enzyme is deeply embedded in the protein.[18–20] Meanwhile, the direct modification of enzyme to the electrode surface can lead to the loss of enzyme activity after curing in a rigid environment. To overcome the above challenges, new materials were used to combine with Cyt c to modify the electrode, which can provide good microenvironment for the electron transfer of enzymes.[21] Zhao *et al.* proposed multi-walled carbon nanotube (MWCNT)-modified electrodes, which promote the direct electron

[a]*School of Biological and Environmental Engineering, Hunan Key Laboratory of Applied Environmental Photocatalysis, Hunan Collaborative Innovation Center of Environmental and Energy Photocatalysis, Changsha University, Changsha, 410022, China. E-mail: hs879314@126.com; Fax: +86 731 84261506; Tel: +86 731 84261506*

[b]*School of Chemistry and Materials Engineering, Huizhou University, Huizhou 516007, China*

[c]*College of Materials and Chemical Engineering, Key Laboratory of Inorganic Nonmetallic Crystalline and Energy Conversion Materials, China Three Gorges University, Yichang, 443002, China. E-mail: cynh1119@163.com; Fax: +86 717 6397505; Tel: +86 717 6397505*

transfer (DET) of Cyt c.[22] However, there are some defects, such as the instability of the prepared electrode caused by physical adsorption. Fortunately, carboxyl/MWCNTs can not only improve the problem through electrostatic adsorption without extra crosslinking agent, but also further increased the loading of Cyt c owing to its larger specific surface area than MWCNTs. More significantly, it is worth exploring that the electrochemical performance of Cyt c-carboxyl/MWCNTs for nitrite detection.

Metal–organic framework (MOF) has attracted much attention since its appearance.[23] As a kind of porous crystal material with three-dimensional network structure formed by coordination of transition metals and organic ligands, MOF has ultrahigh specific surface area and porosity, flexible and controllable structure, which has potential application prospects in many fields (catalysis, energy storage, luminescence, drug delivery and sensor).[24–27] To overcome its low conductivity, Shu *et al.* developed an electrochemical biosensor using MOF combining with AuNPs and CNTs, which exhibited an enhanced electrochemical performance owing to the synergistic effect.[28] However, in order to meet the stability and sensitivity of nitrite detection and ensure that Cyt c-carboxyl/MWCNTs can give full play to its catalytic effect on nitrite, a large platform and stable electrode modification are necessary. Therefore, cobalt MOF (Co-MOF) and gold nanoparticles (AuNPs) were selected as electrode modifiers. Co-MOF with three-dimensional structure possessed large specific surface area and provided a large platform for electrodepositing gold nanoparticles (AuNPs) and loading Cyt c-carboxyl/MWCNTs. Furthermore, the electrodeposition of AuNPs on the Co-MOF *via* Au–NH bound increased the stability and also provided for numerous binding sites for Cyt c-carboxyl/MWCNTs.

In this work, an electrochemical biosensor based on Co-MOF/AuNPs and Cyt c-MWCNTs was constructed for the detection of nitrite (Scheme 1). Firstly, Co-MOF was modified on the glass carbon electrode (GCE), which provided a large specific surface area for electrodeposition of AuNPs. Subsequently, Cyt c/MWCNTs was immobilized on the electrode surface *via* the Au–NH bond between Cyt c and electrode. Particularly, Cyt c could be electrostatically adsorbed with carboxyl groups in functionalized MWCNTs, which improved the dispersion of MWCNTs. Attributed to the synergistic effect of the above nanocomposites and Cyt c, the modified electrode for nitrite detection has excellent electrochemical performance.

2. Experimental

2.1 Materials

$NaNO_2$ was ordered from Tianli Chemical Reagent Co., Ltd. (Tianjin, China). Cytochrome c (Cyt c) and 2-aminoterephthalic acid (NH_2-BDC, 99%) were bought from Shanghai YuanYe Bio-Technology Co., Ltd. (Shanghai, China). Multi-walled carbon nanotubes (MWCNTs) were bought from Beijing Gaoke Technology Material Co., Ltd. (Beijing, China). Chloroauric acid ($HAuCl_4$) was provided by Shanghai Aladdin Biochemical Technology Co., Ltd. (Shanghai, China). 98% sulfuric acid (H_2SO_4) and phosphate buffer saline (PBS) (pH 7.2) were purchased from Tianjin Kemiou Chemical Reagent Co., Ltd. (Tianjin, China). All chemicals and reagents were of analytical grade. Double distilled water was used throughout.

2.2 Apparatus

Transmission electron microscopy (TEM) image was obtained with a HT7700 transmission electron microscope from Japan Hitachi Co., Ltd. (Tokyo, Japan). Scanning electron microscope (SEM) was obtained with a Quanta FEG250 scanning electron microscope from America FEI Co., Ltd. (Hillsboro, America). Ultraviolet spectrophotometer (UV-vis) absorption spectra was recorded using a UV-6100s Double beam spectrophotometer (Mapada, Shanghai, China).

Electrochemical measurements including cyclic voltammetry (CV), electrochemical impedance spectroscopy (EIS) and differential pulse voltammetry (DPV) were conducted with a CHI660E workstation. Wherein, three-electrode system consisted modified GCE working electrode, Ag/AgCl reference electrode containing saturated KCl, platinum wire counter electrode.

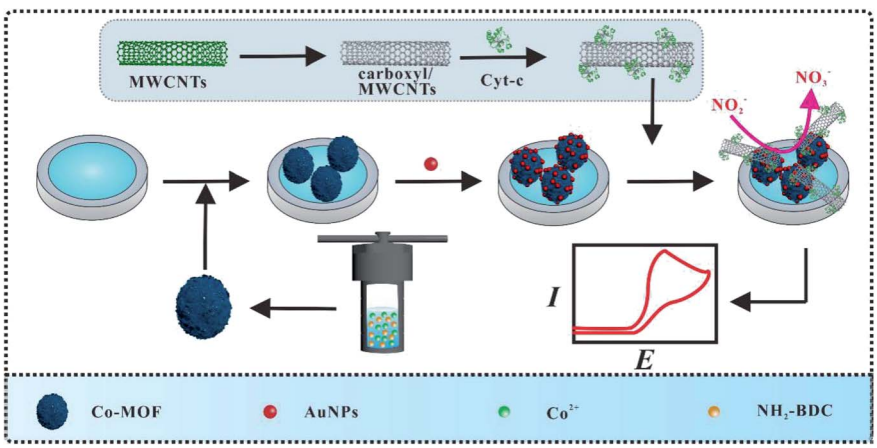

Scheme 1 Schematic diagram of modified electrode preparation and nitrite detection.

2.3 Preparation of Cyt c-MWCNTs

The synthesis of Cyt c-MWCNTs was performed in the following manner.[21] Firstly, MWCNTs were placed in concentrated nitric acid and sulfuric acid (3 : 1). After ultrasonic stirring for 5 h, they were filtered and washed to neutral. Carboxyl/MWCNTs was obtained after drying in vacuum. Subsequently, 1 mg of carboxyl/MWCNTs was added to a 0.060 mg mL^{-1} Cyt c solution. Ultrasonic stirring was performed for 5 min in the ice bath. The supernatant was removed by centrifugation at 12 000 rpm for 15 min to obtain the Cyt c-MWCNTs.

2.4 Preparation of Co-MOF

Co-MOF was synthesized according to literatures.[29,30] 0.2138 g of $Co(NO_3)_2 \cdot 6H_2O$, 0.0815 g NH_2-BDC and 4 mL of DMF were added to the beaker. The mixture was placed in an oil bath pot heated at 140 °C for 20 min after ultrasonic 15 min. After that, the products were centrifuged and washed by DMF and acetonitrile. Then, Co-MOF was dried at 60 °C and stored for further treatment. The resultant Co-MOF was immersed in 10 mL methanol for 36 h and methanol needed to be replaced every four hours. After centrifuging and drying at 60 °C, 1 mg Co-MOF was dispersed in 1 mL distilled water to obtain 1 mg mL^{-1} Co-MOF dispersion.

2.5 Fabrication of biosensor

Before modification, GCE should be polished by using 0.05 μm Al_2O_3 powder for 1 min, and washed ultrasonically with acetone and distilled water, respectively. The GCE can be obtained after the above electrode was dried. Subsequently, 2 μL of Co-MOF was dropped on the surface of GCE. Following that, modified electrode was immersed in 1% $HAuCl_4$ for deposition at −1.2 V for 20 s to obtain AuNPs/Co-MOF/GCE. Finally, 20 μL of Cyt c-MWCNTs was casted on the resultant electrode. Each step above shall be cleaned and dried with distilled water to reduce physical adsorption. Cyt c/GCE, Cyt c/AuNPs/Co-MOF/GCE, Cyt c-MWCNTs/Co-MOF/GCE and Cyt c-MWCNTs/AuNPs/GCE were prepared by the similar procedure.

2.6 Sausage and apple sample analysis

Sausage and apple were obtained from local supermarkets (Zhengzhou, Henan Province, China). Various quantities of nitrite were spiked into 10-fold diluted sausage and apple sample. Sausage and apple sample analysis were conducted by the DPV method.

3. Results and discussion

3.1 Characterization of Co-MOF and Cyt c-MWCNTs

In order to characterize the morphology of the Co-MOF and Cyt c-MWCNTs, TEM and SEM were recorded in Fig. 1. As shown in Fig. 1A, it was observed that Co-MOF had lamellar structure, which provided more active sites and larger specific surface area. Fig. 1B was the SEM of Cyt c-MWCNTs. The prepared Cyt c-MWCNTs were evenly distributed and closely connected. But Fig. 1C showed that the MWCNTs without Cyt c was unevenly dispersed and agglomerated. The above comparison showed that the addition of Cyt c could effectively avoid the agglomeration of MWCNTs.

UV-vis can be used to characterize the conformational changes of Cyt c and its interaction with other compounds. As shown in Fig. 1D, curve a, b and c corresponded to the UV-vis diagrams of Cyt c, MWCNTs and Cyt c-MWCNTs, respectively. Curve a showed that natural Cyt c had strong absorption band

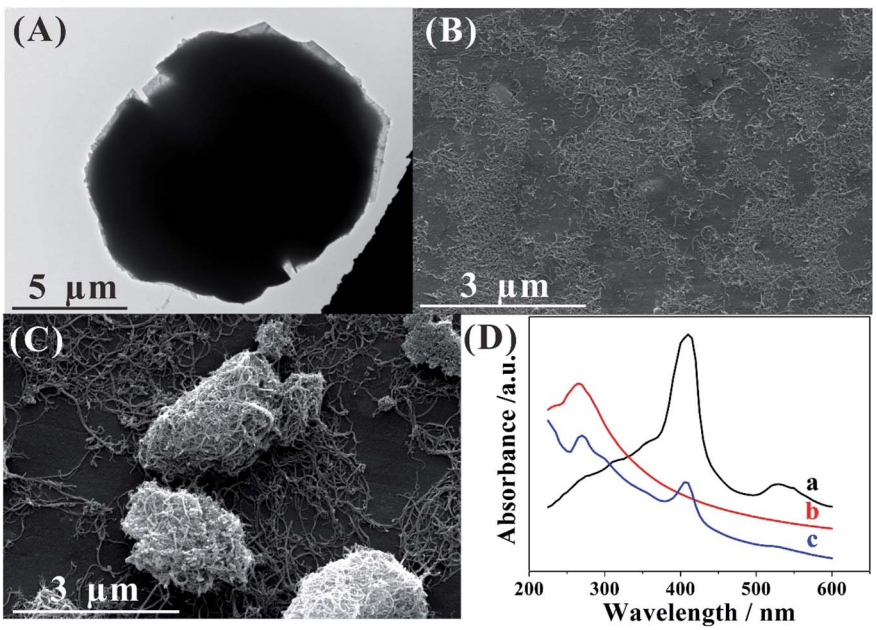

Fig. 1 The characterization of nanomaterials: (A) TEM image of Co-MOF. (B) SEM image of Cyt c-MWCNTs and (C) SEM image of MWCNTs. (D) UV-vis diagrams of Cyt c (a), MWCNTs (b) and Cyt c-MWCNTs (c).

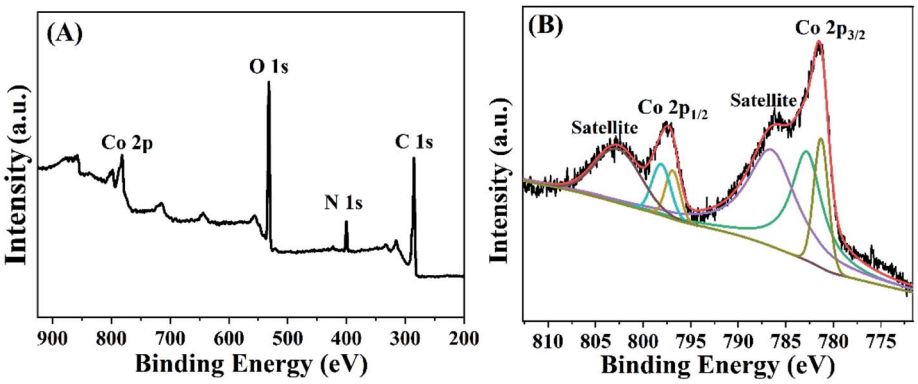

Fig. 2 (A) XPS pattern of Co-MOF. (B) High-resolution Co $2p_{3/2}$ and Co $2p_{1/2}$ XPS spectra of Co-MOF.

at 410 nm and weak absorption band at 530 nm caused by porphyrin chromophore.[31] Curve b showed that there was a characteristic absorption peak at 263 nm.[32] Compared with curve a and b, curve c showed that the Q absorption band disappeared at 530 nm, which illustrated that the soret absorption band of cyt c was blue shifted. In addition, there was a characteristic absorption peak of Cyt c at 408 nm and MWCNTs at 265 nm, which indicated that Cyt c was successfully bound on the surface of MWCNTs.

3.2 X-ray photoelectron spectroscopy characterization of Co-MOF

X-ray photoelectron spectroscopy (XPS) is a powerful tool to investigate the chemical composition of sensing materials.[33,34] Fig. 2A is the XPS survey spectrum for Co-MOF, which verifies that the Co-MOF contained Co, O, N and C elements. Similar as the previous literature,[35] the existence of the peaks of N 1s spectra corresponded to $-NH_2$, which facilitate the deposition of AuNPs *via* Au–NH bound. Furthermore, in order to investigate the chemical composition of Co element in Co-MOF, high-resolution Co $2p_{3/2}$ and Co $2p_{1/2}$ were analyzed (Fig. 2B). The results showed that there were two peaks at 781.5 and 797.6 eV corresponding to Co $2p_{3/2}$ and Co $2p_{1/2}$, respectively, which illustrated that Co-MOF had a high content of Co^{2+}/Co^{3+}. Above results demonstrated that Co-MOF had been successfully synthesized.

3.3 Electrochemical characterization

EIS was used to characterize the interface changes during electrode modification using $[Fe(CN)_6]^{3-/4-}$ as electrochemical probe. Fig. 3 showed the EIS of electrochemical biosensor after stepwise modification, which got the impedance (R_{et}) by fitting. The Ret of bare GCE was 215.5 Ω (curve b). Compared to bare GCE, the R_{et} of Cyt c/GCE increased significantly to 512.2 Ω (curve a), because Cyt c was a bad conductor of electrons. The R_{et} of the prepared Cyt c/AuNPs/GCE (curve c) was significantly reduced to 124.2 Ω when AuNPs were modified on the electrode surface by electrodeposition, which was because AuNPs can significantly accelerate the electron transfer rate and increase the conductivity of Cyt c/AuNPs/GCE. However, after Co-MOF modification, the R_{et} of Cyt c/AuNPs/Co-MOF/GCE (curve d) was reduced to 75.9 Ω. It indicated that the high specific area and active site of Co-MOF increased the AuNPs loading on the electrode surface, thereby increasing the conductivity of the modified electrode and decreasing the R_{et}. When MWCNTs was modified, the R_{et} of the prepared Cyt c-MWCNTs/AuNPs/Co-MOF/GCE (curve e) was further reduced. The EIS diagram showed a straight line in all frequency ranges, with a resistance of 30.42 Ω. It indicated that the reaction process of the electrode was controlled by diffusion and the resistance was small. Moreover, the conductivity of this sensor was further enhanced due to the synergistic effect between the materials. Based on the above results, the R_{et} after stepwise modification changed as expected.

3.4 Electrochemical behavior

The direct electrochemical behavior of different electrodes was studied based on CV. Fig. 4 showed the CV response of different modified electrodes in 0.05 M PBS solution. Compared to bare GCE (curve a), there was tiny peak when Cyt c was modified on the electrode surface (curve b). However, the modification of AuNPs did not significantly increase the current (curve c). After

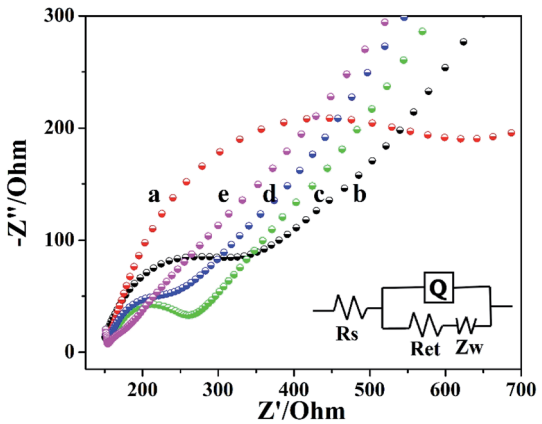

Fig. 3 EIS plots of different electrodes prepared. (a) Cyt c/GCE, (b) GCE, (c) Cyt c/AuNPs/GCE, (d) Cyt c/AuNPs/Co-MOF/GCE, (e) Cyt c-MWCNTs/AuNPs/Co-MOF/GCE (EIS was measured in 10 mM $[Fe(CN)_6]^{3-/4-}$ containing 0.1 M KCl).

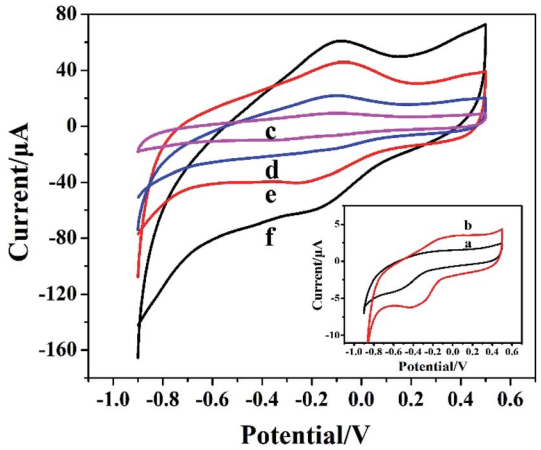

Fig. 4 CV plots of different modified electrodes in 0.05 M PBS. (a) GCE, (b) Cyt c/GCE, (c) Cyt c/AuNPs/GCE, (d) Cyt c-MWCNTs/Co-MOF/GCE, (e) Cyt c-MWCNTs/AuNPs/GCE, (f) Cyt c-MWCNTs/AuNPs/Co-MOF/GCE.

Cyt c-MWCNTs/AuNPs/GCE was prepared successfully, an obvious characteristic peak was observed (curve e). More than that, Cyt c-MWCNTs/Co-MOF/GCE (curve d) also showed a strong characteristic peak. The comparison of the above Cyt c peaks showed that the addition of Cyt c-MWCNTs could fix Cyt c on the electrode surface and made Cyt c retain the activity of its enzyme and produce reversible redox reaction. Moreover, the redox peak on Cyt c-MWCNTs/AuNPs/Co-MOF/GCE was the most prominent (curve f). The results showed that Co-MOF provided a large specific surface area for the immobilization of AuNPs and Cyt c-MWCNTs. Meanwhile, AuNPs and MWCNTs had good conductivity and biocompatibility, which greatly improved the electron transfer efficiency.

3.5 Electrochemical properties for Cyt c-MWCNTs/AuNPs/Co-MOF/GCE

The effect of scan rate on the electrochemical behavior of Cyt c-MWCNTs/AuNPs/Co-MOF/GCE was investigated by CV method. As shown in Fig. 5A, the current increased with scan rate increased, which manifested that the irreversibility of the electrode process increased. From Fig. 5B, the oxidation peak current of Cyt c was linearly correlated with the square root of scan rate in the range of 0.02–0.25 V s^{-1} with a linear equation of $I(\mu A) = -9.3 \times 10^{-5} + 8.62 \times 10^{-4}\nu^{1/2}$ (V s^{-1}) and a correlation coefficient (R^2) of 0.96. Results showed that the reaction process of Cyt c in the Cyt c-MWCNTs/AuNPs/Co-MOF/GCE was controlled by diffusion. Fig. 5C showed that the reduction peak

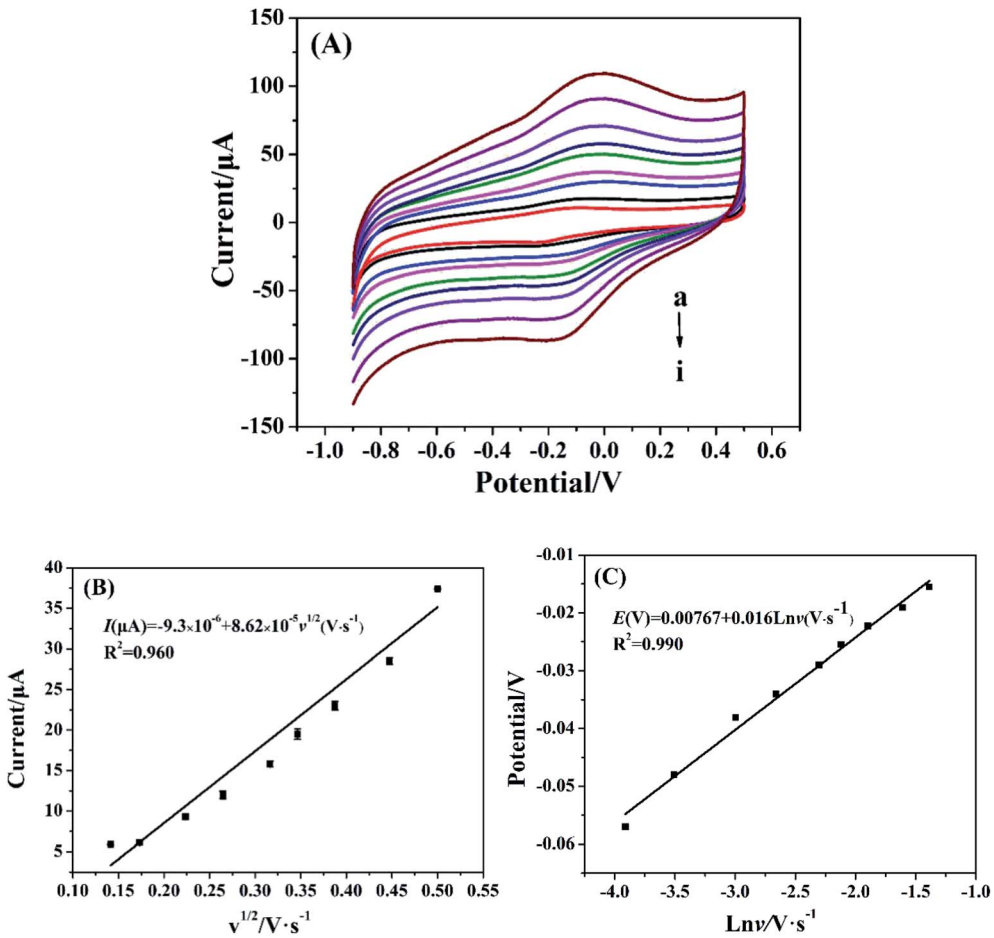

Fig. 5 (A) CV plots of Cyt c-MWCNTs/AuNPs/Co-MOF/GCE at different scan rates (0.02, 0.03, 0.05, 0.07, 0.1, 0.12, 0.15, 0.2 and 0.25 V s^{-1}) in 50 mM PBS. (B) Linear relationship of CV peak current *vs.* square root of scan rate. (C) Linear relationship of oxidation peak potential *vs.* logarithm of scan rate.

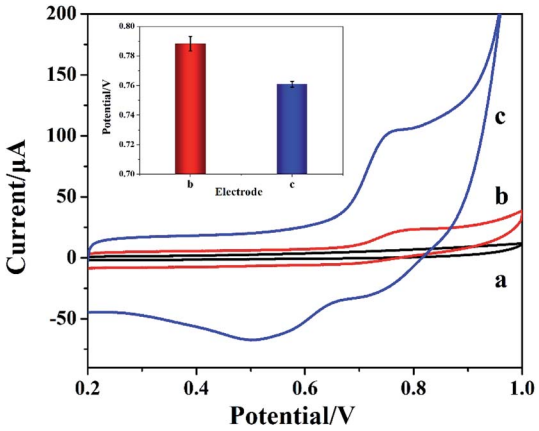

Fig. 6 CV plots of different electrodes. (a) Cyt c-MWCNTs/AuNPs/Co-MOF/GCE in blank solution, (b) GCE in 1 mM nitrite and (c) Cyt c-MWCNTs/AuNPs/Co-MOF/GCE in 1 mM nitrite. The inset was the quantification of peaks appearing on the CV plots ($n = 3$).

potential shifted negatively and the oxidation peak potential shifted positively with the increase of scan rate. Moreover, the oxidation peak potential was linearly correlated with the logarithm of scan rate. The linear equation was E_{pa} (V) = 0.00767 + 0.0160 ln ν (V s^{-1}), $R^2 = 0.985$. According to the Laviron theory:

$$\mathrm{Lg}\, k_s = 2.3RT/(1-\alpha)nF \quad (1)$$

where α is the electron transfer coefficient, n is the number of electron transfers, ν is the scan rate, R is the gas constant, T is temperature and F is Faraday constant. The values of R, T and F were 8.314 J K^{-1} mol^{-1}, 298 K and 96 485 C mol^{-1}, respectively. Based on the relationship between the peak potential and the scan rate, and $E_{p/2} - E_p = 1.875(RT/\alpha F)$, α is 0.59 and n is 1. Results indicated that the oxidation reaction of Cyt c in the Cyt c-MWCNTs/AuNPs/Co-MOF/GCE was a single electron transfer process.

3.6 Electrocatalytic activity of Cyt c-MWCNTs/AuNPs/Co-MOF/GCE for nitrite

The electrocatalytic properties of different electrodes for nitrite were investigated by CV method. Fig. 6 is the CV diagram of 50 mM PBS solution (pH 7.4) before and after adding nitrite with different electrodes. Compared with the blank solution (curve a), a weak oxidation peak at 0.794 V was observed on the CV diagram when 1 mM target was measured using bare GCE (curve b). An obvious oxidation peak appeared at 0.763 V using Cyt c-MWCNTs/AuNPs/Co-MOF/GCE to detect the 1 mM target (curve c), indicating that Cyt c-MWCNTs/AuNPs/Co-MOF/GCE had an obvious catalytic effect on the electrochemical detection of nitrite. The catalytic mechanism was put forward by Geng *et al.*[36] The specific steps are as follows:

$$Fe^{2+}\text{–Cyt c} \rightarrow Fe^{3+}\text{–Cyt c} + e^- \quad (2)$$

$$Fe^{3+}\text{–Cyt c} \rightarrow [Fe^{4+}\text{–Cyt c}]^{\bullet} + 2e^- \quad (3)$$

$$[Fe^{4+}\text{–Cyt c}]^{\bullet} + NO_2^- + H_2O \rightarrow Fe^{3+}\text{–Cyt c} + NO_3^- + 2H^+ \quad (4)$$

3.7 Effect of pH and AuNPs electrodeposition time

Based on Cyt c-MWCNTs/AuNPs/Co-MOF/GCE, the effect of pH on the performance of nitrite detection was investigated by DPV method. As shown in Fig. 7A, the oxidation current of nitrite changed with the pH changed, and its peak current reached its maximum value when pH was 7.4. When pH was higher or lower than 7.4, the peak current significantly decreased. Even if the above modified electrode was re-immersed in the solution of pH 7.4, there was no obvious change in the peak current. It indicated that acidic or alkaline solution could induce conformational change, even degeneration and deactivation of Cyt c, and its effect was irreversible. It can be seen that Cyt c had the largest catalytic activity for nitrite at pH 7.4. Therefore, the pH optimization result was 7.4.

Since AuNPs modified electrode had strong conductivity and good biocompatibility, it could provide a powerful microenvironment for Cyt c. The effect of Cyt c-MWCNTs/AuNPs/Co-MOF/GCE prepared by electrodeposition time of AuNPs (10 s, 20 s, 30 s, 40 s and 50 s) on the electrocatalytic performance of nitrite was investigated by DPV method. Fig. 7B showed that the current increased significantly when the electrodeposition time changed from 10 s to 20 s, which because the increase of electrodeposition time of AuNPs could further promote the immobilization of more

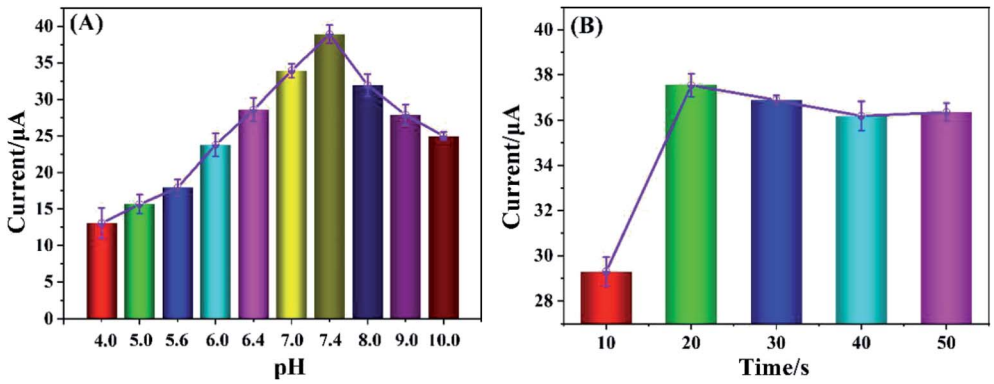

Fig. 7 (A) Peak current *vs.* pH of 1 mM nitrite measurement using Cyt c-MWCNTs/AuNPs/Co-MOF/GCE (pH: 4.0, 5.0, 5.6, 6.0, 6.4, 7.0, 7.4, 8.0, 9.0 and 10). (B) Optimization of electrodeposition time of AuNPs (10, 20, 30, 40 and 50 s).

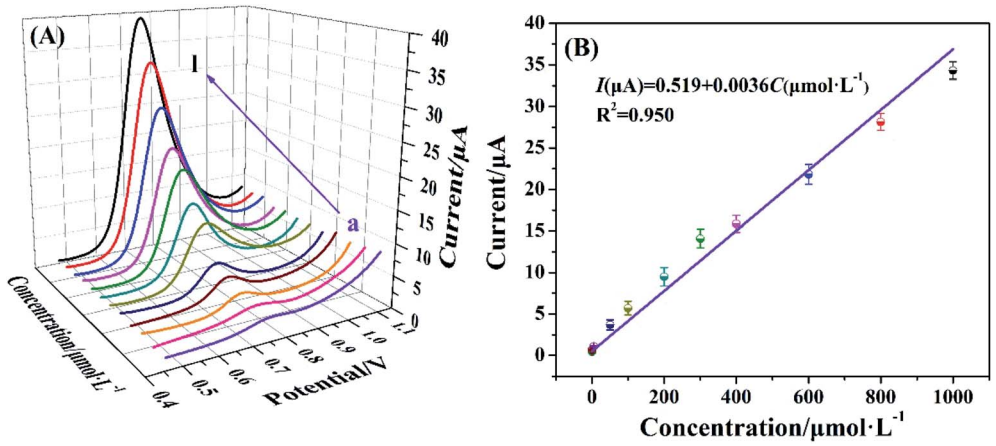

Fig. 8 (A) DPV response of the biosensor for the detection of different concentrations of nitrite (a to i: 0.005, 0.05, 0.1, 5.0, 50.0, 100, 200, 300, 400, 600, 800 and 1000 μmol L^{-1}). (B) Calibration curve of the biosensor ($n = 3$).

Table 1 Comparison of Cyt c-MWCNTs/AuNPs/Co-MOF/GCE with other sensors for nitrite determination

Method	Modified electrode	Linear range (μmol L^{-1})	Limit of detection (μmol L^{-1})	Reference
AMP	NanoAu-MoS_2/GCE	10–2100	0.09	15
CV	Single-layer graphene nanoplatelet (SLGnP)-protein composite film	50–2500	10	37
DPV	RGO/$MnFe_2O_4$/polyaniline	0.05–12 000	0.015	38
AMP	PEDOT/PEDOT-SH/Au	0.15–1000, 1000–16 000	0.051	39
AMP	Cu^{2+}–Cu^{+}/biochar/GCE	1.0–300	0.63	40
DPV	Cyt c-MWCNTs/AuNPs/Co-MOF/GCE	0.005–1000	0.0044	This work

Cyt c-MWCNTs and enhanced the catalytic ability of Cyt c-MWCNTs/AuNPs/Co-MOF/GCE to nitrite. However, when the deposition time was more than 20 s, the AuNPs reached saturation and the amount of Cyt c-MWCNTs did not change significantly. Therefore, the electrodeposition time of 20 s was selected for subsequent experiments.

3.8 Determination of nitrite

In this study, the quantitative analysis performance of nitrite by Cyt c-MWCNTs/AuNPs/Co-MOF/GCE was conducted by DPV method. As shown in Fig. 8A, the corresponding DPV peak current also increased when the concentration of nitrite increased from 5.0×10^{-9} mol L^{-1} to 1.0×10^{-3} mol L^{-1} under optimal conditions. As shown in Fig. 8B, DPV peak current and concentration of nitrite were linearly correlated. The linear equation was $I(\mu A) = 0.519 + 0.0036C$ (μmol L^{-1}), $R^2 = 0.95$, and the detection limit was 4.4×10^{-9} mol L^{-1}. The comparison of Cyt c-MWCNTs/AuNPs/Co-MOF/GCE with other sensors (Table 1) showed that the performance of the Cyt c-MWCNTs/AuNPs/Co-MOF/GCE was superior to other sensors.

3.9 Reproducibility, stability and effect of interferences on the determination of nitrite

The reproducibility and stability of electrodes were very important for energy conservation, environmental protection and the development of commercial products. The same concentration of nitrite was detected using the five prepared Cyt c-MWCNTs/AuNPs/Co-MOF/GCE in 0.05 M PBS (pH 7.4), and the RSD was 3.6%. Similarly, the same concentration of nitrite was detected 5 times using the same Cyt c-MWCNTs/AuNPs/Co-MOF/GCE, and the RSD was 3.6%. The same concentration of nitrite was detected using six prepared Cyt c-MWCNTs/AuNPs/Co-MOF/GCE after different storage time, and the RSD was 4.2%. All of these results showed that Cyt c-MWCNTs/AuNPs/Co-MOF/GCE had good reproducibility and stability.

The anti-interference ability of Cyt c-MWCNTs/AuNPs/Co-MOF/GCE against possible organic and inorganic materials was

Table 2 Determination of nitrite in real samples by the proposed biosensor

Sample	Added (μmol L^{-1})	Found[a] (μmol L^{-1})	Recovery (%)	RSD (%, $n = 3$)
Sausage	50	47.60 ± 1.68	95.20	3.53
	200	196.00 ± 8.80	98.00	4.51
	400	394.00 ± 18.90	98.50	4.80
Apple	50	49.40 ± 2.40	98.80	4.84
	100	94.60 ± 3.30	95.00	3.51
	200	191.10 ± 8.30	95.60	4.37

[a] Average of three replicate measurements.

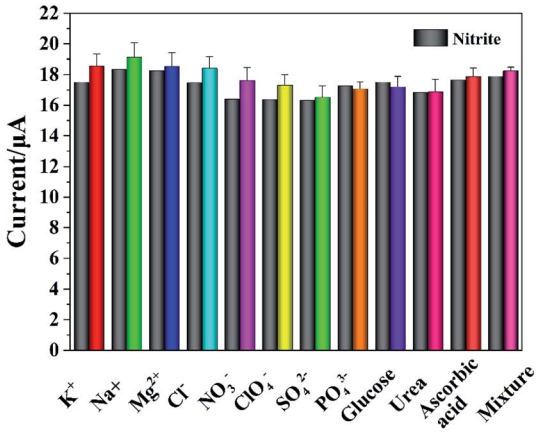

Fig. 9 Effect of interferents on the detection of nitrite by Cyt c-MWCNTs/AuNPs/Co-MOF/GCE.

studied by DPV method. 100 times concentration of K^+, Na^+, Mg^{2+}, Cl^-, SO_4^{2-}, PO_4^{3-}, NO_3^-, ClO_4^-, 10 times concentration of ascorbic acid, glucose and uric acid were added to 500 μM nitrite. According to previous literatures,[41,42] a mixed sample (the concentration of interference in the mixture is the same as that of individual interference) should also be studied. The response currents of Cyt c-MWCNTs/AuNPs/Co-MOF/GCE before and after the addition of interferers were compared. The experimental results were shown in Fig. 9, and the RSD was all less than 5% with no significant influence, indicating that the prepared Cyt c-MWCNTs/AuNPs/Co-MOF/GCE had high selectivity.

3.10 Determination of real samples

In order to investigate the performance of the electrode in real samples, recovery experiments were conducted using the standard addition method in sausage and apple samples (purchased from the Zhengzhou local supermarket). The results are shown in Table 2, the recovery rate is 95.0%–98.8%. It showed that this method could effectively detect nitrite in real samples.

4. Conclusions

In conclusion, a novel electrochemical biosensor based on Co-MOF/AuNPs and Cyt c-MWCNTs was constructed for the detection of nitrite. Co-MOF/AuNPs provided a large specific surface area for the immobilization of Cyt c/MWCNTs. Cyt c-MWCNTs possessed good biocompatibility and superior electrocatalytic activity towards nitrite. Compared with other nitrite biosensors, the prepared Cyt c-MWCNTs/AuNPs/Co-MOF/GCE possessed excellent electrochemical properties including high electron transfer efficiency and electrocatalytic activity. In addition, the biosensor showed a low detection limit and high selectivity. This study provided a novel approach for the detection of nitrite.

Conflicts of interest

The authors declare that they have no competing interests.

Acknowledgements

This work was supported by the Initial Founding of Scientific Research for the Introduction of Talents of Changsha University (Grant No. SF1814), the Professorial and Doctoral Scientific Research Foundation of Huizhou University (Grant No. 2018JB034), the 111 Project (Grant No. D20015) and Research Foundation of Yichang Science and Technology Bureau (Grant No. A19-302-04).

References

1 C. Hui, X. Guo, P. Sun, R. A. Khan, Q. Zhang, Y. Liang and Y.-H. Zhao, *Bioresour. Technol.*, 2018, **248**, 146–152.
2 Y. Zhang, Y. Zhao, S. Yuan, H. Wang and C. He, *Sens. Actuators, B*, 2013, **185**, 602–607.
3 K. Zhao, H. Song, S. Zhuang, L. Dai, P. He and Y. Fang, *Electrochem. Commun.*, 2007, **9**, 65–70.
4 Y. G. Huang, J. D. Ji and Q. N. Hou, *Mutat. Res.*, 1996, **358**, 7–14.
5 N. S. Bryan, D. D. Alexander, J. R. Coughlin, A. L. Milkowski and P. Boffetta, *Food Chem. Toxicol.*, 2012, **50**, 3646–3665.
6 D. M. West, R. Mu, S. Gamagedara, Y. Ma, C. Adams, T. Eichholz, J. G. Burken and H. Shi, *Environ. Sci. Pollut. Res.*, 2015, **22**, 8594–8602.
7 Q.-H. Wang, L.-J. Yu, Y. Liu, L. Lin, R.-g. Lu, J.-p. Zhu, L. He and Z.-L. Lu, *Talanta*, 2017, **165**, 709–720.
8 M. Shariati-Rad, M. Irandoust and S. Mohammadi, *Spectrochim. Acta, Part A*, 2015, **149**, 190–195.
9 S. Chamandust, M. R. Mehrasebi, K. Kamali, R. Solgi, J. Taran, F. Nazari and M.-J. Hosseini, *Int. J. Food Prop.*, 2016, **19**, 1983–1993.
10 J. Zhao, J. Wang, Y. Yang and Y. Lu, *J. Chromatogr. Sci.*, 2015, **53**, 1169–1177.
11 L. Wang, J. Chen, H. Chen, C. Zhou, B. Ling and J. Fu, *J. Lumin.*, 2011, **131**, 83–87.
12 L. Luo, S. Ma, L. Li, X. Liu, J. Zhang, X. Li, D. Liu and T. You, *Food Chem.*, 2019, **292**, 98–105.
13 Y. Li, J. He, J. Chen, Y. Niu, Y. Zhao, Y. Zhang and C. Yu, *Biosens. Bioelectron.*, 2018, **101**, 7–13.
14 M. Sentic, S. Arbault, L. Bouffier, D. Manojlovic, A. Kuhn and N. Sojic, *Chem. Sci.*, 2015, **6**, 4433–4437.
15 X. Li, N. Zou, Z. Wang, Y. Sun, H. Li, C. Gao, T. Wang and X. Wang, *Chem. Pap.*, 2020, **74**, 441–449.
16 F. Farivar, A. A. Moosavi-Movahedi, Y. Sefidbakht, K. Nazari, J. Hong and N. Sheibani, *Biochem. Eng. J.*, 2010, **49**, 89–94.
17 R. Radi, J. F. Turrens and B. A. Freeman, *Arch. Biochem. Biophys.*, 1991, **288**, 118–125.
18 Q. Xu, C. Mao, N.-N. Liu, J.-J. Zhu and J. Sheng, *Biosens. Bioelectron.*, 2006, **22**, 768–773.
19 S. Ma and R. Ludwig, *ChemElectroChem*, 2019, **6**, 958–975.
20 R. del Cano, L. Mateus, G. Sanchez-Obrero, J. Manuel Sevilla, R. Madueno, M. Blazquez and T. Pineda, *Talanta*, 2018, **176**, 667–673.
21 M. Murphy, K. Theyagarajan, G. Prabusankar, S. Senthilkumar and K. Thenmozhi, *Appl. Surf. Sci.*, 2019, **492**, 718–725.

22 H.-Z. Zhao, Q. Du, Z.-S. Li and Q.-Z. Yang, *Sensors*, 2012, **12**, 10450–10462.
23 S. Li and F. Huo, *Nanoscale*, 2015, **7**, 7482–7501.
24 M. Zhao, S. Ou and C.-D. Wu, *Acc. Chem. Res.*, 2014, **47**, 1199–1207.
25 A. R. Millward and O. M. Yaghi, *J. Am. Chem. Soc.*, 2005, **127**, 17998–17999.
26 L. Heinke, M. Tu, S. Wannapaiboon, R. A. Fischer and C. Woell, *Microporous Mesoporous Mater.*, 2015, **216**, 200–215.
27 D. Liu, R. C. Huxford and W. Lin, *Angew. Chem., Int. Ed.*, 2011, **50**, 3696–3700.
28 Y. Shu, Q. Lu, F. Yuan, Q. Tao, D. Jin, H. Yao, Q. Xu and X. Hu, *ACS Appl. Mater. Interfaces*, 2020, **12**, 49480–49488.
29 X. Yang, J. Lv, Z. Yang, R. Yuan and Y. Chai, *Anal. Chem.*, 2017, **89**, 11636–11640.
30 Z. Wang, H. Yu, J. Han, G. Xie and S. Chen, *Chem. Commun.*, 2017, **53**, 9926–9929.
31 J. Petrovic, R. A. Clark, H. Yue, D. H. Waldeck and E. F. Bowden, *Langmuir*, 2005, **21**, 6308–6316.
32 Y. Liu, L. Yu, S. Zhang, J. Yuan, L. Shi and L. Zheng, *Colloids Surf., A*, 2010, **359**, 66–70.
33 M. Wang, M. Hu, Z. Li, L. He, Y. Song, Q. Jia, Z. Zhang and M. Du, *Biosens. Bioelectron.*, 2019, **142**, 111536.
34 Y. Song, M. Xu, Z. Li, L. He, M. Hu, L. He, Z. Zhang and M. Du, *Sens. Actuators, B*, 2020, **321**, 128527.
35 L. Dai, Y. Li, Y. Wang, X. Luo, D. Wei, R. Feng, T. Yan, X. Ren, B. Du and Q. Wei, *Biosens. Bioelectron.*, 2019, **132**, 97–104.
36 R. Geng, G. Zhao, M. Liu and M. Li, *Biomaterials*, 2008, **29**, 2794–2801.
37 R. Yue, Q. Lu and Y. Zhou, *Biosens. Bioelectron.*, 2011, **26**, 4436–4441.
38 S. Sahoo, P. K. Sahoo, A. Sharma and A. K. Satpati, *Sens. Actuators, B*, 2020, **309**, 127763.
39 Y. Ge, R. Jamal, R. Zhang, W. Zhang, Z. Yu, Y. Yan, Y. Liu and T. Abdiryim, *Microchim. Acta*, 2020, **187**, 248.
40 L. Cao, Z.-W. Kang, Q. Ding, X. Zhang, H. Lin, M. Lin and D.-P. Yang, *Sci. Total Environ.*, 2020, **723**, 138008.
41 Y. Song, M. Xu, Z. Li, L. He, M. Hu, L. He, Z. Zhang and M. Du, *Sens. Actuators, B*, 2020, **311**, 127927.
42 F. Duan, C. Guo, M. Hu, Y. Song, M. Wang, L. He, Z. Zhang, R. Pettinari and L. Zhou, *Sens. Actuators, B*, 2020, **310**, 127844.